APPLIED SCIENCES AND ENGINEERING

Optimization principles and the figure of merit for triboelectric generators

Jun Peng,[1]* Stephen Dongmin Kang,[1,2]* G. Jeffrey Snyder[1]†

Energy harvesting with triboelectric nanogenerators is a burgeoning field, with a growing portfolio of creative application schemes attracting much interest. Although power generation capabilities and its optimization are one of the most important subjects, a satisfactory elemental model that illustrates the basic principles and sets the optimization guideline remains elusive. We use a simple model to clarify how the energy generation mechanism is electrostatic induction but with a time-varying character that makes the optimal matching for power generation more restrictive. By combining multiple parameters into dimensionless variables, we pinpoint the optimum condition with only two independent parameters, leading to predictions of the maximum limit of power density, which allows us to derive the triboelectric material and device figure of merit. We reveal the importance of optimizing device capacitance, not only load resistance, and minimizing the impact of parasitic capacitance. Optimized capacitances can lead to an overall increase in power density of more than 10 times.

INTRODUCTION

Rubbing two different materials is a charge-generating method as old as the discovery of electricity itself. Attempts to produce electricity from this triboelectric method has led to modern instruments such as the Van de Graaff generator (*1*), which is for sourcing an extremely high voltage. Today, with the renewed interest in energy harvesting for distributed power sources, triboelectric generators are gaining interest as an alternative source. Many variants of application schemes have been demonstrated or conceptualized recently (*2*–*17*) and described as triboelectric nanogenerators (*18*) in pioneering work, leading to deepened interest in understanding their power and efficiency (*19*–*25*). Nevertheless, power optimization schemes are still premature where, often, only the load resistance is adjusted with lack of a general principle for full optimization. Furthermore, the impact of device imperfections (*23*) tends to be discussed in less detail despite its significant influence on device operation.

Here, we concisely model the contact-separation mode generator and reveal that the output power could be increased substantially by optimizing the capacitance in addition to the load resistance. Matching the resistance-capacitance (*RC*) product to the characteristic frequency of the triboelectric process is essential to use the mechanical motion and effectively convert it into electrical power. An added capacitor is necessary to stabilize the *RC* product because the total capacitance varies during the cycle. Adjusting resistance alone leads to poor matching conditions and, thus, low power.

We also model how parasitic capacitance, which is practically inevitable, affects the performance of the device. We show that proper adjustments to minimize the ineffectiveness caused by parasitic capacitance could also lead to a substantial increase in output power. We anticipate that, with the power improvement strategies learned from our model analysis, triboelectric generators could be a competitive energy-harvesting source.

[1]Department of Materials Science and Engineering, Northwestern University, Evanston, IL 60208, USA. [2]Department of Applied Physics and Materials Science, California Institute of Technology, Pasadena, CA 91125, USA.
*These authors contributed equally to this work.
†Corresponding author. Email: jeff.snyder@northwestern.edu

RESULTS

Using the triboelectric effect

Triboelectricity is best known for forming charges on a material surface upon contact or rubbing. Although a pair of oppositely charged surfaces are essential for triboelectric power generation, the analysis described below shows that it is the motion of these electrostatic charges (not their production itself) that leads to useful electric power.

Any two different surfaces put into contact will exchange charge as determined by their Fermi level of electrons [see the study of Matsusaka *et al.* (*26*) for a review on detailed complexities]. The Fermi level relative to the vacuum level is known as the work function of a material. Materials with a high work function are more electronegative and easily accept electrons from a lower–work function (electropositive) material. Therefore, a larger difference in work function drives more charge exchange. As the charges exchange, they create an electrostatic potential difference, which tends to pull them together, thus creating a contact potential at the point of contact that exactly counteracts the work function difference.

Like a parallel plate capacitor, the electrostatic potential $V = \sigma \cdot d/\varepsilon$ between surface charges is the product of surface charge density σ and charge separation distance d (relative to permittivity ε). When the surfaces touch, charge separation distance is smallest and, thus, σ is largest. As the surfaces separate, the electric field increases rapidly, pushing the charges back to their original material. If the materials have sufficient conductivity, these charges flow through points still in contact during the separation process (Fig. 1). In insulators, where charges are not as free to move, some surface charge density remains after the surfaces are completely separated. As these fixed surface charges are pulled apart, mechanical work against the force of attraction is required. This work is what is converted into electrical energy observed at the load. It is the electrostatic induction of these residual surface charges that can account for all the electrical currents and voltages observed in an external circuit.

Device operation and its optimization

Because the interfacial charge transfer is not involved in the external circuit, we only need to consider the steady-state total surface charge σS (S is the surface area) that remains to analyze the generation cycle

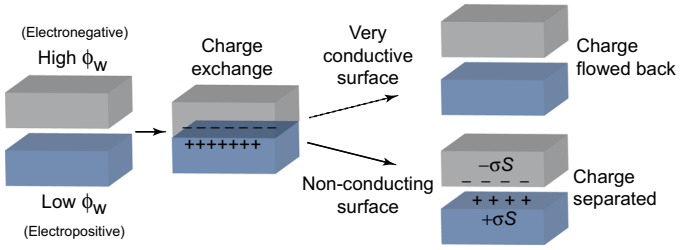

Fig. 1. Triboelectric charge generation. Two materials with different work functions ϕ_w exchange electrons when brought into contact, generating surface charges. Rubbing is not essential as long as intimate contact is made. When the two materials separate, an electrostatic voltage is produced, which establishes a force to move the charges back if there is any conducting path. When at least one of the materials is not conductive at the surface, surface charges remain after the separation.

during the operation. Any charge loss due to leakage through the dielectric, although reducing efficiency, is replenished with the new contact at every cycle, and a steady state surface charge is established.

Triboelectric generators have a generation mechanism involving a periodic mechanical motion that separates the triboelectrically established surface charge σS and induces a change in the electric potential between electrodes. The changed electrical potential induces a flow of charge (dQ/dt) through a load resistor, which could be used as electrical energy. Because mechanical energy is converted into electrical potential energy at the same time energy is being extracted (decreases the potential), the optimization of generation is inherently related to matching the frequency or time scales of these two processes. In short, the mechanical motion should "resonate" with the electrical energy removal. It is expected from this general understanding that the optimization of a device will involve tuning circuit elements (which changes the characteristic time of charge response) to match a specific mechanical motion or mode.

The most effective way to do mechanical work by separating charged flat surfaces is to separate them in the direction perpendicular to the surface, as depicted in Fig. 2A. For this process to be effective throughout a cycling motion, the frequency of the mechanical motion (ω) should match the characteristic frequency of the circuit ($1/RC_{total}$). However, most types of triboelectric generators (including variants of the contact-separation mode and lateral sliding mode) have a time-varying capacitance; the dielectric layer and air gap sandwiched between metals altogether acts as a capacitor, and the mechanical motion changes the distance between the two surfaces and, thus, the total capacitance. This time-varying RC product is why the generated current is, in general, not in phase with the mechanical motion and, thus, not most effective [unless the generator is designed to have a constant capacity, such as the freestanding mode (*27*)].

The time variance of the RC product can be reduced to better match the mechanical driving motion over the entire cycle. We compare Fig. 2B, where the device has a thick dielectric layer (or large $1/C_{device}$), to Fig. 2C, where the device has a thin dielectric layer (or small $1/C_{device}$). For a given mechanical motion, the change in the overall RC product is much less when $1/C_{device}$ is large, which leads to better matching. As a result, the charge motion with respect to time (Fig. 2D) becomes a smoother function similar to that of the driving motion, from which mechanical energy is converted more effectively. The strategy for reducing the time variance of the RC product for better matching is applicable to any type of triboelectric generator with a varying capacitance.

The trade-off for using a large $1/C_{device}$ for good overall matching is that one needs a larger load resistance R_L to match a similar $1/RC = \omega$. Figure 2E shows the decrease in current due to the requirement of a larger R_L for matching.

As a result, power generation is optimized when both C_{device} and R_L are balanced (Fig. 2F). As one departs from the optimum, it is generally advantageous to have better matching rather than higher currents (Fig. 2F), which highlights the importance of good matching. This concept of optimizing both R and C is in contrast to the dominant literature that optimizes only the load resistance to find maximum power while keeping the device at a large C_{device} (poor matching). C_{device} can be tuned not only by changing the dielectric thickness but also by adding a series capacitor to the circuit. Using a simple model, we demonstrate how this simple two-element optimization (R_L and C_{device}) can lead to output power many times higher than conventional operating conditions.

Model for triboelectric power generation

We study the most basic form of triboelectric generation, the contact-separation mode, which could be the basis for analyzing other variations. As long as the generation involves a mechanical motion, which forms a steady-state generation cycle with a characteristic frequency, the scaling behavior should be generally applicable to other types of triboelectric generators.

Device parameters that could be experimentally controlled are numerous, including the maximum separation distance, mechanical frequency, dielectric surface area, load resistance, and capacitance. These parameters form a prohibitively large phase space with interdependencies, making it difficult to devise a general strategy and define a figure-of-merit for the maximum power density of triboelectric generation.

Using a general modeling approach, the large number of device parameters can be combined into a few dimensionless quantities that guide the effectiveness of power generation. We find two, but only two, independently adjustable parameters—dimensionless resistance and capacitance—which can be optimized for the maximum power output. We show through the scaling properties of the dimensionless parameters that our results could be applied to both nanogenerators and larger-scale generators. Practical limitations causing reduced effectiveness or efficiency can be understood in terms of departure from the ideal model.

Theoretical maximum power and figure of merit

Our interest is in the elemental driving motion, which is a sinusoidal motion that changes the air gap x as a function of time

$$x = \frac{x_{max}}{2}(1 - \cos \omega t) \quad (1)$$

We assume that the two electrodes (moving and stationary) of area S form an ideal capacitor where a charge σS gives a voltage V across the capacitor with capacitance C, where $V = \sigma S/C$. Here, C is due to the dielectric layer and the air gap. Electrical power is extracted from a load resistance in series (Fig. 2).

During the initial contact ($x = 0$), opposite charges will be produced on the contacting surfaces. Because we are interested in the steady-state power production, we assume that a total surface charge of $-S\sigma$ remains constant on the dielectric layer surface and that it represents the steady-state surface charge. In the electrodes, a charge Q is transferred back and forth between the moving and stationary electrode (through

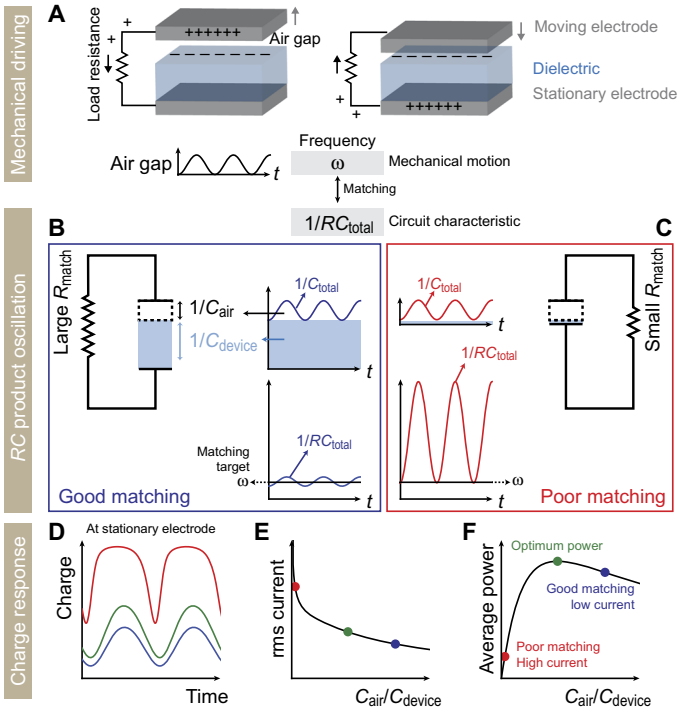

Fig. 2. Principles for optimizing triboelectric generation. (**A**) Schematic of a typical triboelectric generator (contact-separation mode). The dielectric maintains a surface charge throughout the cycle. When the moving electrode pulls away from the dielectric and enlarges the air gap (left), charge separation builds a potential that drives some of the charge to the stationary electrode. A load resistor is placed between the electrodes to produce work from this charge motion. The moving electrode cycles back and forth, producing an alternating current. The mechanical motion is characterized by an angular frequency ω. (**B**) A device circuit scheme where the device $1/RC$ is maintained close to ω. The device $1/C_{device}$ is large, making the relative fluctuation in $1/C_{total} = 1/C_{air} + 1/C_{device}$ smaller. A large load resistance is used to compensate for the large $1/C_{device}$. (**C**) A device circuit scheme where overall matching is poor. $1/C_{device}$ is small, resulting in a large fluctuation in $1/RC$. (**D**) The charge deposited in the stationary electrode. The good matching case (blue) resembles a sinusoid, whereas the poor matching case (red) is highly distorted. (**E**) The overall current decreases with larger $1/C_{device}$ because of the requirement of a larger load resistor. (**F**) The time-averaged power is optimized with a balance of both good matching and current. Power is generally higher with good matching rather than with high current.

the load resistor) due to the electrical potential change that accompanies the change in x, eventually reaching a periodic oscillation in steady state. In this ideal system, charge is not lost or dissipated, and triboelectric charge generation need not be considered at steady state.

Combining these principles results in a dimensionless differential equation describing the charge in the stationary electrode (see the Supplementary Materials)

$$R^*\frac{dQ^*}{d\theta} + Q^*\left(\frac{1}{C^*} + x^*\right) = x^* \tag{2}$$

Here, $\theta = \omega t$ is the phase of the driving motion; $Q^* = Q/S\sigma$ is the dimensionless charge in the stationary electrode, which is a fraction of the total surface charge $S\sigma$; and $x^* = x/x_{max}$ is the fractional air gap that sinusoidally varies between 0 and 1. The dimensionless capacitance C^* and load resistance R^* are the only two independent variables that characterize the system

$$R^* \equiv \frac{R_L \omega \varepsilon_0 S}{x_{max}} \tag{3}$$

$$C^* \equiv \frac{C_{device}}{C_{air}} \tag{4}$$

where R_L is the load resistance, ε_0 is the permittivity of vacuum, C_{device} is the capacitance of the entire device when the air gap is closed (that is, includes the dielectric layer and also any additional capacitor connected in series), and $C_{air} = \varepsilon_0 S/x_{max}$ is the capacitance of the maximum air gap. The governing equation is identical when the moving electrode surface has an additional dielectric layer (*19*).

The power output is characterized by the averaged dimensionless power

$$\overline{P^*} \equiv \frac{1}{2\pi}\int_{cycle} I^{*2} R^* \tag{5}$$

where $I^* = dQ^*/d\theta$.

By solving for the steady-state solution of Eq. 2 (see the Supplementary Materials), we find how the power output is optimized with respect to R^* and C^* (Fig. 3). It is seen that the maximum condition for $\overline{P^*}$ is pinpointed at one particular condition

$$\begin{aligned} R^* &= 1.14 \\ 1/C^* &= 0.82 \\ 2\pi\overline{P^*} &= 0.127 \end{aligned} \tag{6}$$

This condition, together with Eqs. 3 and 4, specifies how the real physical parameters should be optimized. For instance, for a lower-frequency driving motion (small ω), one would need either a larger load resistance or a larger device area; if two different sets of physical parameters yield the same R^* and C^*, they specify identical device operation conditions.

Real power density (time-averaged) can be calculated by scaling $\overline{P^*}$

$$\frac{\bar{P}}{S} = \overline{P^*}\cdot\frac{\sigma^2 \omega x_{max}}{\varepsilon_0} \quad (W/m^2) \tag{7}$$

which offers the definition for a "device figure of merit" for power density in contact-separation mode by setting $\overline{P^*}$ to its maximum value

$$FOM_{device} = 0.064\cdot\frac{\sigma^2 \bar{v}}{\varepsilon_0} \quad (W/m^2) \tag{8}$$

FOM_{device} is the maximum power density obtainable from the contact-separation generator. Note that $\bar{v} = \omega x_{max}/\pi$ is the average speed of the mechanical motion. It is seen that the only material-related parameter in the FOM_{device} is the steady-state surface charge density,

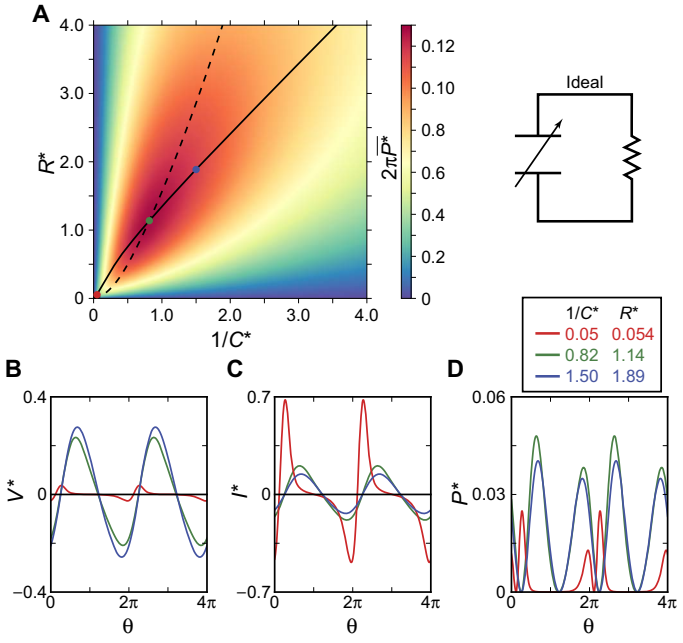

Fig. 3. Analysis of the ideal model in steady state with dimensionless parameters. (**A**) Power map for the two device parameters R^* and $1/C^*$. The color represents the dimensionless power per cycle $2\pi\overline{P^*}$. Restricted optimization of power for a given $1/C^*$ (solid line) and a given R^* (dashed line) is shown, and the two coincide at the global optimum condition (green dot). Two example suboptimal conditions (red dot, poor matching case; blue dot, good matching case) are indicated. (**B**) V^* (= $I^* R^*$), (**C**) I^*, and (**D**) P^* curves for the global optimum condition and two suboptimal conditions indicated in (A). It is seen that the poor matching condition (red lines) produces highly distorted curves with low power, whereas the good matching condition (blue lines) shows characteristics as good as the global optimum condition (green lines).

which leads to the definition of the "material figure of merit" for power density

$$\mathrm{FOM}_{\mathrm{mater}} = \sigma^2 \quad (\mathrm{C}^2/\mathrm{m}^4) \tag{9}$$

To keep the number more tractable, one could also use a normalized material figure of merit

$$\mathrm{FOM}^{\mathrm{n}}_{\mathrm{mater}} = \frac{\sigma^2}{\varepsilon_0} \quad (\mathrm{J}/\mathrm{m}^3) \tag{10}$$

Note that $\mathrm{FOM}_{\mathrm{mater}}$ is a surface property dependent on which material it is brought into contact with. $\mathrm{FOM}_{\mathrm{mater}}$ coincides to what has been established in the study of Zi *et al.* (*21*).

We next show an example of power density estimation using typical device parameters. We assume a generator with $\sigma = 12\ \mu\mathrm{C}/\mathrm{m}^2$, $x_{\max} = 1$ mm, and $w = 2\pi \times 60$ Hz. Then, the maximum power density obtainable with a fully optimized generator is $\mathrm{FOM}_{\mathrm{device}} = 124\ \mathrm{mW}/\mathrm{m}^2$. In a conventional device scheme where only the dielectric layer of thickness d is used without an additional series capacitor, $1/C^* = d/\varepsilon_r x_{\max}$ (ε_r is relative permittivity). In this case, $1/C^*$ is typically < 0.05 (that is, $d < 150\ \mu$m for $\varepsilon_r = 3$), at which the maximum power density is only 23 mW/m^2, more than five times lower than the $\mathrm{FOM}_{\mathrm{device}}$.

The above example illustrates how the device capacitance has a significant impact on the output power, an aspect that has been mostly overlooked in the recent literature. Increasing $1/C^*$ toward the global optimum can be done not only by using a thicker dielectric layer but also by adding a capacitor in series to the dielectric layer: $1/C_{\mathrm{device}} = 1/C_{\mathrm{dielectric}} + 1/C_{\mathrm{series}}$.

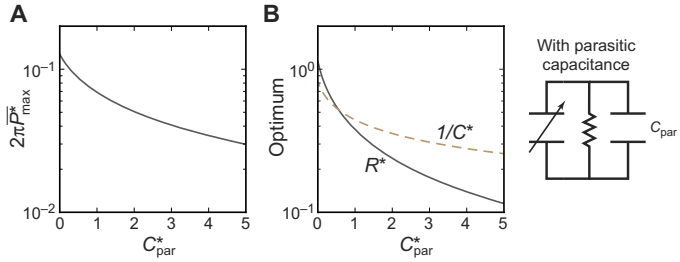

Fig. 4. The influence of parasitic capacitance. (**A**) Decrease in the maximum obtainable power with increasing dimensionless parasitic capacitance C^*_{par}. (**B**) Shift in the optimum R^* (solid line) and $1/C^*$ (dashed line) condition with the presence of C^*_{par}.

Partly similar conclusions regarding the relevant parameters have been reached in the literature (for example, regarding σ^2 or $\bar{v}$) (*19*, *21*); however, earlier reports have based their model analysis on the transient behavior (in the transient state, the power output could be instantaneously high at nonoptimal conditions; see the Supplementary Materials); the literature tends to focus on a restricted optimization only based on load resistance (or sometimes no load conditions), leading to disparate conclusions regarding power output and optimization.

Zi *et al.* (*21*) offered one of the first dedicated discussions on the figure of merit for triboelectric nanogenerators by considering an upper bound for power output constructed with a combined cycle of open-circuit (potential buildup) and short-circuit (instantaneous discharge) processes. Open-circuit voltages and short-circuit charges were used to define a figure of merit. However, from the perspective of designing a device, it is more convenient to have a figure of merit that could be estimated just with the design parameters rather than with output characteristics. Furthermore, the practical output limit at a load resistor is much lower than what can be calculated from the instantaneous discharge process. The $\mathrm{FOM}_{\mathrm{device}}$ we propose is the actual maximum power density one could obtain at the load resistor under optimized capacitance and no parasitic reduction.

Power reduction due to parasitic capacitance

An important factor causing a deviation from the ideal case will be the presence of parasitic capacitance in the circuit. It is a small but unavoidable element that always exists in an electric circuit. In triboelectric generators, the parasitic capacitance can easily be comparable to that of the generator, significantly affecting the power output and the optimum device parameters (*23*). This leakage mechanism can be modeled with an additional capacitor in parallel to the device (Fig. 4). Then, instead of the charge produced from the triboelectric effect always going through the load resistor, part of it leaks into C_{par}. This leakage affects the effectiveness (but not efficiency) of generating power, slowing down the energy conversion rate.

Parasitic leakage is characterized with the dimensionless parasitic capacitance

$$C^*_{\mathrm{par}} \equiv \frac{C_{\mathrm{par}}}{C_{\mathrm{air}}} = \frac{C_{\mathrm{par}} x_{\max}}{\varepsilon_0 S} \tag{11}$$

where C_{par} is the real parasitic capacitance.

By solving for the steady-state solution (see the Supplementary Materials), we find how the output power is reduced with increasing parasitic capacitance (Fig. 4A). For example, assume x_{max} = 1 mm and S = 22 cm^2, yielding C_{air} = 20 pF. Then, a parasitic capacitance of 20 pF indicates C^*_{par} = 1, which reduces the maximum output power to 54 % of the FOM_{device}. The optimum R^* and $1/C^*$ also downshift with C_{par} (Fig. 4B).

Increasing the area of the metal-dielectric interface is the best way to minimize the impact of a given parasitic capacitance. To decrease C^*_{par} for a given C_{par}, one can either increase S or decrease x_{max}(Eq. 11); however, because x_{max} is directly proportional to the device figure of merit (Eq. 8), only increasing S is beneficial. Therefore, larger-area generators are much more robust to parasitic leakage.

DISCUSSION

Comparison to experiments

Our model shows good agreement with the experimental data reported by Niu *et al.* (*19*). We compare the power generation curve with respect to load resistance. For the data set where the device capacitance was not varied, the corresponding model curve is a vertical cross section of Fig. 3 (also see fig. S3). It is seen in Fig. 5A that the curve shapes from three different driving speeds all fit well to a fixed curve shape given by $1/C^* = 0.07$.

Because the maximum power conditions for the three different driving speeds in the data set are expected to be described with identical dimensionless parameters (that is, a set of $1/C^*$ and R^*), the maximum power and optimal load resistance in real dimensions are expected to scale with respect to average speed as compared in Fig. 5B. The small deviations are thought to be associated with parasitic capacitance, which was not possible to be accounted for with the given information.

Parasitic capacitance seems to explain the power scaling observed with respect to an increase in x_{max}. Niu *et al.* (*19*) increased x_{max} by five times, which increases the FOM_{device} by the same factor. However, the observed power increase was limited to a factor of 2.3. Note that for a given parasitic capacitance, C^*_{par} scales with x_{max} (Eq. 11); that is, the influence of parasitic capacitance increases. As a result, the benefit of increased x_{max} is diminished.

Regarding the material figure of merit, several experimental reports have demonstrated the significance of σ^2 (*28*–*31*). For quantitative assessment of the scaling behavior with respect to σ^2, power output at the load resistance should be measured while taking into account the $1/C^*$ of the generator.

Conversion efficiency

Because the power production in a triboelectric generator is purely by electrostatic induction, the energy conversion efficiency of this process itself is 100%. It can be confirmed (see the Supplementary Materials) with our model that the power output is exactly equal to the net work done by the mechanical motion, which is true, in general, even for non-optimal R^* and $1/C^*$ and a finite C^*_{par}.

Loss of efficiency originates from other imperfections rather than from the electrostatic conversion process or purely capacitive leakage. For example, the surface charge on the dielectric layer could leak through the film, which is equivalent to resistive loss. This type of loss can be minimized by keeping the dielectric film resistance much larger than the load resistor. Frictional losses regarding the mechanical motion or the charge exchange process (during the contact of two surfaces) are other sources of losses that could be important.

Practical requirements in implementing the generator could also lead to reduced efficiency. The 100% conversion efficiency of the electrostatic induction is by considering the net mechanical work, including both positive (during separation of charged surfaces) and negative (while joining the charged surfaces back together) work input. In applications where negative work could not be meaningful, the relevant efficiency would have to be calculated with only the positive work input. This alternative definition gives 45 % efficiency for the maximum power condition (see the Supplementary Materials). Another example is when the load is not simply a load resistor. Then, there would be losses associated with power conditioning (*32*) to convert the output into a "useful" form.

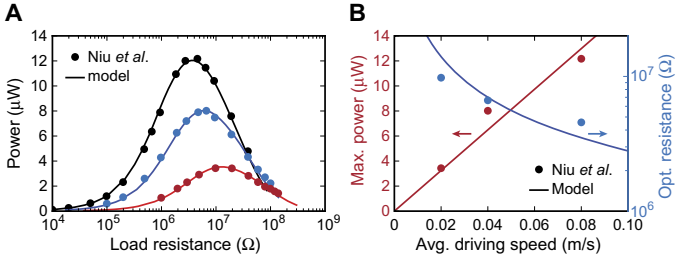

Fig. 5. Model fitting to experimental data from Niu *et al.* (*19*). (**A**) Power change with respect to load resistance. Experimental data sets consist of driving conditions with average speeds of 0.08 m/s (black circles), 0.04 m/s (blue circles), and 0.02 m/s (red circles). Solid lines are from the ideal model by assuming a fixed $1/C^* = 0.07$, which determines the shape of the curve. The scaling of the model curve to real dimensions was determined by fitting due to the lack of experimental details in the study of Niu *et al.* (*19*). (**B**) The change of maximum power (left axis) and optimum resistance (for a fixed device capacitance; right axis) with respect to the average driving speed. The curves represent the expected scaling behavior of maximum power ($\propto \bar{v}$, Eq. 7) and optimum load resistance ($\propto 1/\omega$ for fixed x_{max}, Eq. 3) from the ideal model.

CONCLUSIONS

Triboelectric generators make use of the surface charge maintained in an insulating material during the repeated contact and separation of a dissimilar material. Electrostatic induction due to the separation of two charged surfaces builds a potential that drives a current through the load.

Power generation is more effective when the time-varying RC product of the generator better matches the mechanical motion frequency during the cycle. A larger $1/C_{device}$ is beneficial for good matching but reduces the current level. Generally, the power output characteristic is more stable in the good matching regime (high $1/C_{device}$), which could be achieved by connecting a series capacitor to the circuit.

The device figure of merit (Eq. 8) determines the maximum output power density obtainable from a generator at steady state. Here, the only material-related parameter is surface charge density, which defines the material figure of merit.

Parasitic capacitance reduces the power generation effectiveness. Enlarging the surface area of the dielectric-metal interface can minimize power reduction due to parasitic capacitances. The fundamentals of triboelectric generation presented in this paper could lead to designs of more sophisticated applications and help to establish triboelectric generators as an attractive energy-harvesting source.

METHODS

Model differential equations were found by constructing circuit diagrams equivalent to the generator device. The governing equation was reduced to have a minimum number of independent variables equal to the degrees of freedom. Steady-state solutions were found analytically, which were numerically evaluated for model analysis. Details can be found in the Supplementary Materials.

SUPPLEMENTARY MATERIALS

Supplementary material for this article is available at http://advances.sciencemag.org/cgi/content/full/3/12/eaap8576/DC1

fig. S1. Circuit model diagrams of triboelectric generators.
fig. S2. Transient characteristics of the ideal model.
fig. S3. One-dimensional projections of the steady-state dimensionless power output.
fig. S4. The influence of parasitic capacitance on device characteristics.
fig. S5. Comparison of the output power and mechanical work input.

REFERENCES AND NOTES

1. R. J. van de Graaff, J. G. Trump, W. W. Buechner, Electrostatic generators for the acceleration of charged particles. *Rep. Prog. Phys.* **11**, 1 (1947).
2. Z. L. Wang, Catch wave power in floating nets. *Nature* **542**, 159–160 (2017).
3. A. Li, Y. Zi, H. Guo, Z. L. Wang, F. M. Fernández, Triboelectric nanogenerators for sensitive nano-coulomb molecular mass spectrometry. *Nat. Nanotechnol.* **12**, 481–487 (2017).
4. Y.-C. Lai, J. Deng, S. L. Zhang, S. Niu, H. Guo, Z. L. Wang, Single-thread-based wearable and highly stretchable triboelectric nanogenerators and their applications in cloth-based self-powered human-interactive and biomedical sensing. *Adv. Funct. Mater.* **27**, 1604462 (2017).
5. Y. Zi, J. Wang, S. Wang, S. Li, Z. Wen, H. Guo, Z. L. Wang, Effective energy storage from a triboelectric nanogenerator. *Nat. Commun.* **7**, 10987 (2016).
6. B. Meng, W. Tang, Z.-h. Too, X. Zhang, M. Han, W. Liu, H.-X. Zhang, A transparent single-friction-surface triboelectric generator and self-powered touch sensor. *Energ. Environ. Sci.* **6**, 3235–3240 (2013).
7. X. Li, J. Tao, J. Zhu, C. Pan, A nanowire based triboelectric nanogenerator for harvesting water wave energy and its applications. *APL Mater.* **5**, 074104 (2017).
8. Y. Bao, R. Wang, Y. Lu, W. Wu, Lignin biopolymer based triboelectric nanogenerators. *APL Mater.* **5**, 074109 (2017).
9. W. Xu, L.-B. Huang, M.-C. Wong, L. Chen, G. Bai, J. Hao, Environmentally friendly hydrogel-based triboelectric nanogenerators for versatile energy harvesting and self-powered sensors. *Adv. Energy Mater.* **7**, 1601529 (2017).
10. W. Deng, B. Zhang, L. Jin, Y. Chen, W. Chu, H. Zhang, M. Zhu, W. Yang, Enhanced performance of ZnO microballoon arrays for a triboelectric nanogenerator. *Nanotechnology* **28**, 135401 (2017).
11. S. W. Chen, X. Cao, N. Wang, L. Ma, H. R. Zhu, M. Willander, Y. Jie, Z. L. Wang, An ultrathin flexible single-electrode triboelectric-nanogenerator for mechanical energy harvesting and instantaneous force sensing. *Adv. Energy Mater.* **7**, 1601255 (2017).
12. F.-R. Fan, Z.-Q. Tian, Z. L. Wang, Flexible triboelectric generator. *Nano Energy* **1**, 328–334 (2012).
13. Y. Song, X. Cheng, H. Chen, J. Huang, X. Chen, M. Han, Z. Su, B. Meng, Z. Song, H. Zhang, Integrated self-charging power unit with flexible supercapacitor and triboelectric nanogenerator. *J. Mater. Chem. A* **4**, 14298–14306 (2016).
14. T.-H. Chang, Y.-W. Peng, C.-H. Chen, T.-W. Chang, J.-M. Wu, J.-C. Hwang, J.-Y. Gan, Z.-H. Lin, Protein-based contact electrification and its uses for mechanical energy harvesting and humidity detecting. *Nano Energy* **21**, 238–246 (2016).
15. C. K. Jeong, K. M. Baek, S. Niu, T. W. Nam, Y. H. Hur, D. Y. Park, G.-T. Hwang, M. Byun, Z. L. Wang, Y. S. Jung, K. J. Lee, Topographically-designed triboelectric nanogenerator via block copolymer self-assembly. *Nano Lett.* **14**, 7031–7038 (2014).
16. Q. Liang, X. Yan, Y. Gu, K. Zhang, M. Liang, S. Lu, X. Zheng, Y. Zhang, Highly transparent triboelectric nanogenerator for harvesting water-related energy reinforced by antireflection coating. *Sci. Rep.* **5**, 9080 (2015).
17. H. S. Wang, C. K. Jeong, M.-H. Seo, D. J. Joe, J. H. Han, J.-B. Yoon, K. J. Lee, Performance-enhanced triboelectric nanogenerator enabled by wafer-scale nanogrates of multistep pattern downscaling. *Nano Energy* **35**, 415–423 (2017).
18. Z. L. Wang, J. Chen, L. Lin, Progress in triboelectric nanogenerators as a new energy technology and self-powered sensors. *Energ. Environ. Sci.* **8**, 2250–2282 (2015).
19. S. Niu, S. Wang, L. Lin, Y. Liu, Y. S. Zhou, Y. Hu, Z. L. Wang, Theoretical study of contact-mode triboelectric nanogenerators as an effective power source. *Energ. Environ. Sci.* **6**, 3576–3583 (2013).
20. A. Zhang, W. Liu, Y. Zhang, On the mechanism and optimization of triboelectric nanogenerators. *Nanotechnology* **26**, 425401 (2015).
21. Y. Zi, S. Niu, J. Wang, Z. Wen, W. Tang, Z. L. Wang, Standards and figure-of-merits for quantifying the performance of triboelectric nanogenerators. *Nat. Commun.* **6**, 8376 (2015).
22. T. Jiang, W. Tang, X. Chen, C. B. Han, L. Lin, Y. Zi, Z. L. Wang, Figures-of-merit for rolling-friction-based triboelectric nanogenerators. *Adv. Mater. Technol.* **1**, 1600017 (2016).
23. K. Dai, X. Wang, S. Niu, F. Yi, Y. Yin, L. Chen, Y. Zhang, Z. You, Simulation and structure optimization of triboelectric nanogenerators considering the effects of parasitic capacitance. *Nano Res.* **10**, 157–171 (2017).
24. S. Niu, Y. S. Zhou, S. Wang, Y. Liu, L. Lin, Y. Bando, Z. L. Wang, Simulation method for optimizing the performance of an integrated triboelectric nanogenerator energy harvesting system. *Nano Energy* **8**, 150–156 (2014).
25. S. Niu, Z. L. Wang, Theoretical systems of triboelectric nanogenerators. *Nano Energy* **14**, 161–192 (2015).
26. S. Matsusaka, H. Maruyama, T. Matsuyama, M. Ghadiri, Triboelectric charging of powders: A review. *Chem. Eng. Sci.* **65**, 5781–5807 (2010).
27. S. Niu, Y. Liu, X. Chen, S. Wang, Y. S. Zhou, L. Lin, Y. Xie, Z. L. Wang, Theory of freestanding triboelectric-layer-based nanogenerators. *Nano Energy* **12**, 760–774 (2015).
28. J. W. Lee, H. J. Cho, J. Chun, K. N. Kim, S. Kim, C. W. Ahn, I. W. Kim, J.-Y. Kim, S.-W. Kim, C. Yang, J. M. Baik, Robust nanogenerators based on graft copolymers via control of dielectrics for remarkable output power enhancement. *Sci. Adv.* **3**, e1602902 (2017).
29. H. Ryu, J.-H. Lee, T.-Y. Kim, U. Khan, J. H. Lee, S. S. Kwak, H.-J. Yoon, S.-W. Kim, High-performance triboelectric nanogenerators based on solid polymer electrolytes with asymmetric pairing of ions. *Adv. Energy Mater.* **7**, 1700289 (2017).
30. C. Yao, X. Yin, Y. Yu, Z. Cai, X. Wang, Chemically functionalized natural cellulose materials for effective triboelectric nanogenerator development. *Adv. Funct. Mater.* **27**, 1700794 (2017).
31. S. Wang, Y. Xie, S. Niu, L. Lin, C. Liu, Y. S. Zhou, Z. L. Wang, Maximum surface charge density for triboelectric nanogenerators achieved by ionized-air injection: Methodology and theoretical understanding. *Adv. Mater.* **26**, 6720–6728 (2014).
32. X. Cheng, L. Miao, Y. Song, Z. Su, H. Chen, X. Chen, J. Zhang, H. Zhang, High efficiency power management and charge boosting strategy for a triboelectric nanogenerator. *Nano Energy* **38**, 438–446 (2017).

Acknowledgments

Funding: This work was supported by the Solid State Solar Thermal Energy Conversion Center, an Energy Frontier Research Center, funded by the U.S. Department of Energy, Office of Science, Basic Energy Sciences (DE-SC0001299). **Author contributions:** J.P. performed the background experiments, which inspired the project, and conducted model analysis. S.D.K. constructed the dimensionless models and wrote the manuscript. G.J.S. supervised the project. All authors discussed the results throughout the project and edited the manuscript. **Competing interests:** The authors declare that they have no competing interests. **Data and materials availability:** All data needed to evaluate the conclusions in the paper are present in the paper and/or the Supplementary Materials. Additional data related to this paper may be requested from the authors.

Submitted 3 September 2017
Accepted 17 November 2017
Published 15 December 2017
10.1126/sciadv.aap8576

Citation: J. Peng, S. D. Kang, G. J. Snyder, Optimization principles and the figure of merit for triboelectric generators. *Sci. Adv.* **3**, eaap8576 (2017).

Optimization principles and the figure of merit for triboelectric generators

Jun Peng, Stephen Dongmin Kang and G. Jeffrey Snyder

Sci Adv **3** (12), eaap8576.
DOI: 10.1126/sciadv.aap8576